

# Mass Transport Model for Semiconductor Nanowire Growth

Jonas Johansson,\* C. Patrik T. Svensson, Thomas Mårtensson, Lars Samuelson, and Werner Seifert

*Solid State Physics and The Nanometer Structure Consortium, Lund University, P.O. Box 118, SE-22100 Lund, Sweden*

*Received: April 4, 2005; In Final Form: May 27, 2005*

We present a mass transport model based on surface diffusion for metal-particle-assisted nanowire growth. The model explains the common observation that for III/V materials thinner nanowires are longer than thicker ones. We have grown GaP nanowires by metal-organic vapor phase epitaxy and compared our model calculations with the experimental nanowire lengths and radii. Moreover, we demonstrate that the Gibbs–Thomson effect can be neglected for III/V nanowires grown at conventional temperatures and pressures.

## Introduction

Electronic devices and interconnects based on semiconductor nanowires (or nanowhiskers) are promising for electronics applications. Nanowires offer a way to fabricate devices in a bottom-up approach instead of the conventional top-down methods. Such self-assembly fabrication routes are of great interest for the continued miniaturization of electronics, and nanowires could indeed contribute considerably to the solution of the problem of extending Moore's law further than what is possible with conventional complementary metal oxide semiconductor technology.

Some devices based on semiconductor nanowires have already been demonstrated.<sup>1–4</sup> However, development of such devices requires strict control of the nanowire fabrication process. To achieve such control, it is of the utmost importance to understand the growth mechanism.

At present, there is some confusion in the literature concerning the growth behavior of metal-particle-assisted semiconductor nanowires grown on epitaxial substrates. There is disagreement concerning the nature of the assisting particle—is it a liquid alloy as in the classical description of vapor–liquid–solid (VLS) growth,<sup>5,6</sup> or is it a solid particle, i.e., vapor–solid–solid growth, as has been reported recently?<sup>7,8</sup> In another investigation, it was shown that it is only possible to grow InAs nanowires with metal-organic vapor phase epitaxy (MOVPE) when the Au–In alloy particle is solid.<sup>9</sup> At temperatures where it is liquid, no growth occurred.

There is also a lack of consensus concerning the growth mechanism, especially the role of the Gibbs–Thomson effect on nanowire growth. Referring to this effect, Givargizov<sup>6</sup> explained his observation that thicker wires of Si, grown in the SiCl<sub>4</sub>/H<sub>2</sub> system, grow faster in length than thinner wires. However, most of today's experiments in molecular beam epitaxy (MBE),<sup>10</sup> chemical beam epitaxy (CBE),<sup>11</sup> and MOVPE<sup>12</sup> show the opposite behavior.

The purpose of the present investigation is to explain these different observations concerning the length growth rate versus radius. To do so, we derive a mass transport model for metal-particle-assisted nanowire growth and fit it to experimental

results concerning nanowire lengths and radii. Such a model has in fact already been proposed,<sup>12</sup> but we present the first formal derivation and quantification of the model. Using our model together with in-depth discussions of the role of the Gibbs–Thomson effect, we can attribute the discrepancies concerning length growth rate versus thickness to different supersaturations typically chosen for the different growth systems.

## Experimental Section

Gold aerosol particles with intentionally broad size distributions were deposited<sup>13</sup> on GaP (111)B (i.e., group V terminated {111}) substrates, which had been etched in a solution of 2HCl/2H<sub>2</sub>O/HNO<sub>3</sub> for 20 min in an ultrasonic bath. After gold deposition, the substrates were transferred to a low-pressure MOVPE reactor. Before growth, the gold-particle-strewn samples were annealed at 650 °C for 10 min. After this, the temperature was ramped down to the growth temperature (440, 470, or 500 °C), and trimethyl gallium (TMG) was introduced. The samples were then grown at a total pressure of 100 mbar under a hydrogen carrier gas flow of 6 L/min and a constant flow of phosphine. The molar fractions of phosphine and TMG in the flowing gas were  $7.5 \times 10^{-3}$  and  $1.25 \times 10^{-5}$ , respectively. This results in a V/III ratio of 600, which ensures that phosphine is in excess in the growth chamber. After 4 min of growth, the TMG was turned off, and the samples were cooled under a flow containing phosphine.

Images of the nanowire samples were collected by means of scanning electron microscopy (SEM), allowing values to be obtained for length and radius.

## Diffusion Model

In this section, we describe a mass-transport-limited model for III/V semiconductor nanowire growth. It is a diffusion–deposition model with kinetically hindered growth on the substrate surface and on the sides of the nanowires. In the ideal case, growth occurs only at the interface between the metal particle and the nanowire. This is therefore treated as a sink. This sink creates the driving force for material flow toward the interface. The fundamentals of the model are two diffusion equations, which are interconnected through the adatom flux at the base of the growing nanowire; see Figure 1.

\* Author to whom correspondence should be addressed. Phone: +46 46 2227740. Fax: +46 46 2223637. E-mail: jonas.johansson@ff.lth.se

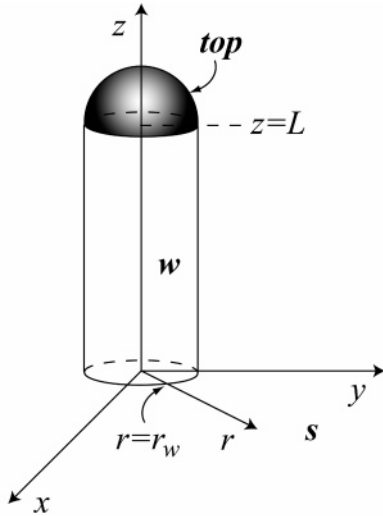


**Figure 1.** Coordinate system used in the calculations. The domains *s* (substrate surface) and *w* (nanowire side wall), where the two diffusion equations are solved, are indicated, as are the top, the radius, and the height ( $z = L$ ) of the nanowire.

The general assumptions of this model are that (i) the metal particle is assumed to be hemispherical, (ii) there is steady-state adatom diffusion on the substrate and nanowire sides toward the metal particle, (iii) the processes within the metal particle (diffusion) as well as at the metal–semiconductor interface (nucleation) need not be considered in detail, and (iv) the interwire separation is fairly large. The model should be general and valid for all materials and growth systems, provided that assumptions i–iv are valid.

Specifically, for III/V nanowires, we treat the group III atoms outside the metal particle as the surface-diffusing, rate-limiting species<sup>14</sup> and assume that the group V atoms are always in excess, which is the common case in MOVPE growth of III/V materials. For our intentions, assumption i should be excellent, but for a more detailed understanding of the metal particle–semiconductor interface, more realistic shapes and contact angles must be considered. From transmission electron microscopy (TEM) investigations, it is in any case known that this interface is atomically flat.<sup>15</sup> Assumption ii is a quasi-static approach, where we assume that the nanowire length growth rate is slow compared to the velocity of the diffusing adatoms. Assumption iii is problematic, since there are clear indications that under certain conditions diffusion through a solid particle<sup>8</sup> or nucleation effects at the interface<sup>10</sup> can be rate-limiting. However, we will neglect such effects inside the particle and focus only on the transport of the precursors toward the particle, i.e., mass transport toward this sink. This assumption should be valid for nanowire growth in MOVPE where nanowires grow 15–30 times faster than in CBE and MBE.

The area number density of adatoms on the substrate surface,  $n_s$ , can be described by the following equation

$$D_s \nabla^2 n_s - n_s / \tau_s + R_s = \partial n_s / \partial t \quad (1)$$

In eq 1,  $D_s$  is the surface diffusivity of adatoms on the substrate,  $\tau_s$  is the average time an adatom diffuses on the substrate, and  $R_s$  is the effective impingement rate of adatoms on the substrate surface, which will be discussed in detail below. For typical growth situations, incorporation dominates over desorption. Therefore, we interpret  $\tau_s$  as the average time an adatom diffuses before being incorporated into the nanowire. For this quantity, it is only possible to estimate an upper limit, which is the average

time required to replace an adatom by an atom from the vapor,  $\tau_s = N_s / R_s$ , where  $N_s$  is the density of surface sites.<sup>16</sup> The Laplacian in eq 1 is given by  $\nabla^2 = \partial^2 / \partial r^2 + r^{-1} \partial / \partial r$ , i.e., polar coordinates with no angular dependence. The bounded, steady-state solution to eq 1, obeying  $n_s(r_w) = 0$ , where  $r_w$  is the radius of the growing nanowire, can be expressed in terms of the modified Bessel function of the second kind,<sup>17</sup>  $K_0(x)$

$$n_s(r) = R_s \tau_s \left[ 1 - \frac{K_0(r / \lambda_s)}{K_0(r_w / \lambda_s)} \right] \quad (2)$$

where we have introduced the surface diffusion length,  $\lambda_s = \sqrt{D_s \tau_s}$ . Note that eq 2 is only valid when assumption iv, which is that the interwire separation is large, is valid. If not, i.e., if the interwire separation is less than  $\lambda_s$ , then individual nanowires compete for the available material, and the adatom density,  $R_s \tau_s$ , is not reached between the nanowires.

The adatom density on the sides of the nanowire,  $n_w$ , is modeled by the one-dimensional diffusion equation

$$D_w \partial^2 n_w / \partial z^2 - n_w / \tau_w + R_w = \partial n_w / \partial t \quad (3)$$

where  $z$  is the length coordinate along the nanowire,  $z = 0$  at the base, and  $z = L$  at the nanowire–metal particle interface; see Figure 1. The symbols  $D_w$ ,  $\tau_w$ , and  $R_w$  in eq 3 denote diffusivity, diffusion time, and deposition rate on the nanowire sides, respectively. The steady-state solution to eq 3, obeying the flux boundary condition at the nanowire base ( $z = 0$ ,  $r = r_w$ ),  $D_w \partial n_w(0) / \partial z = -D_s \partial n_s(r_w) / \partial r = J_{sw}$ , and the density boundary condition at  $z = L$ ,  $n_w(L) = 0$ , is given by

$$n_w(z) = R_w \tau_w \left[ 1 - \frac{\cosh(z / \lambda_w)}{\cosh(L / \lambda_w)} \right] - \frac{J_{sw} \lambda_w \sinh((L - z) / \lambda_w)}{D_w \cosh(L / \lambda_w)} \quad (4)$$

where  $\lambda_w = \sqrt{D_w \tau_w}$  is the diffusion length along the side of the nanowire. Here, it is important to stress that  $\lambda_s$  and  $\lambda_w$  should be seen as effective diffusion lengths or migration lengths, since the mechanisms underlying the movements of the atoms are not understood in detail. The explicit expression for the adatom flux from the surface to the nanowire is given by

$$J_{sw} = -R_s \lambda_s \frac{K_1(r_w / \lambda_s)}{K_0(r_w / \lambda_s)} \quad (5)$$

The length growth rate of the nanowire can be expressed as the adatom flux from the nanowire sides into the metal particle multiplied by the circumference, divided by the cross-sectional area of the nanowire plus the contribution from direct impingement on the metal particle,  $-D_w \partial n_w(L) / \partial z \times 2\Omega / r_w + 2\Omega R_{top}$ , where  $\Omega$  is the atomic (or molecular) volume of the growth species. The mantle area of the metal particle (here modeled as a hemisphere), divided by the cross-sectional area of the nanowire, equals 2; hence this factor appears in the second term in the length growth rate. The amount of material that is solved by the metal particle per unit time will also be incorporated into the nanowire, per unit time, during steady-state growth. An explicit expression for the nanowire length growth rate,  $dL / dt$ , can now be written

$$\frac{dL}{dt} = \frac{2\Omega R_w \lambda_w}{r_w} \tanh(L / \lambda_w) - \frac{2\Omega J_{sw}}{r_w \cosh(L / \lambda_w)} + 2\Omega R_{top} \quad (6)$$

In this equation, the first term represents the diffusion of material

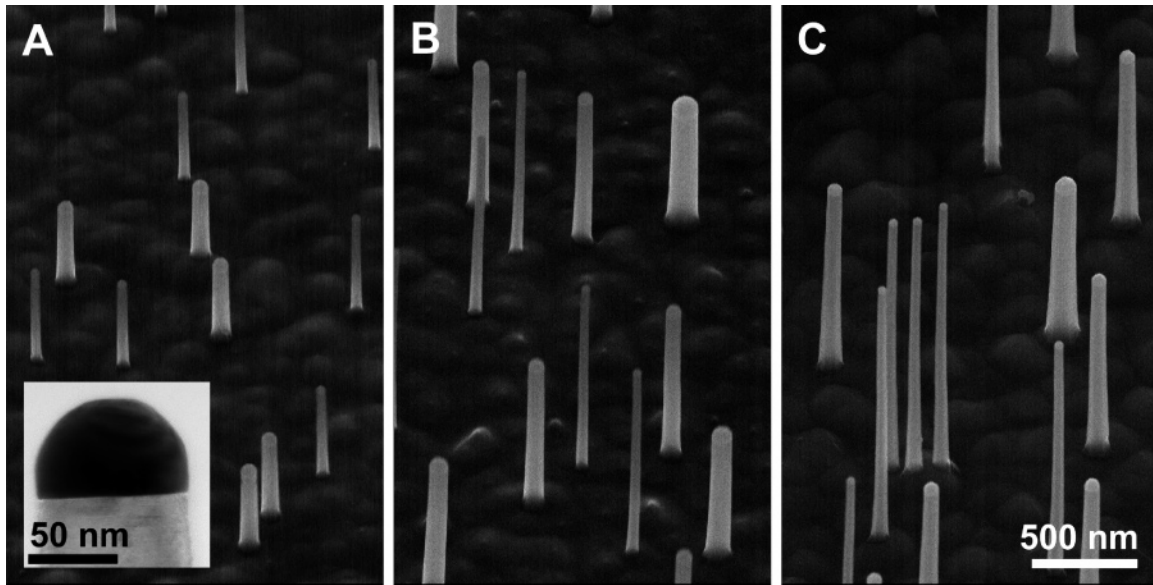


**Figure 2.** Scanning electron micrographs of GaP nanowires grown with MOVPE at different temperatures: (A) 440 °C, (B) 470 °C, and (C) 500 °C. The tilt angle in the SEM was 45°. The scale is the same in all three SEM images. The transmission electron micrograph inset shows the top region of one of the GaP nanowires grown at 440 °C with its roughly hemispherical gold particle.

directly deposited on the nanowire sides, and the second term accounts for adatom diffusion from the substrate surface up along the nanowire. The third term accounts for the material deposited directly on the metal particle.

In the beginning, the growth rate is slow until the metal particle has reached its steady-state supersaturation. While the nanowire grows, the surface contribution decays while the contribution from direct deposition on the nanowire sides increases. Finally, when  $L > \lambda_w$ , the length of the nanowire increases linearly with  $t$ , as has been observed in experiments.<sup>11</sup>

It is interesting to note that at late-stage growth, i.e., when  $L \gg \lambda_w$ , eq 6 becomes

$$\frac{dL}{dt} = 2R \left( 1 + \frac{\lambda_w}{r_w} \right) \quad (7)$$

for  $R = \Omega R_w = \Omega R_{top}$ . This is exactly the same as eq 1 in the work by Seifert et al.,<sup>12</sup> where only deposition on the nanowire sides and metal particle was considered to contribute to the growth.

## Results and Discussion

In Figure 2, we show SEM images of the MOVPE-grown GaP nanowires. From these micrographs, it is clearly visible that the thinner nanowires are longer than the thicker ones. We see also that the length of the nanowires increases with increasing temperature. There is, however, a limited temperature interval for nanowire growth. At too low temperatures, the nanowires bend, and a single wire can subsequently grow in different directions. This behavior is not yet completely understood, but a possible explanation may be that the growth front directly under the gold particle becomes rough. This is a common problem in epitaxy at low temperatures. Our lowest temperature, 440 °C, is just above the low-temperature limit. At too high temperatures, growth on the substrate surface is no longer kinetically hindered, and the competition from substrate growth dominates. Our highest temperature, 500 °C, is slightly below this limit.

In Figure 3, we quantify the results seen in Figure 2. The experimentally obtained individual nanowire lengths are plotted

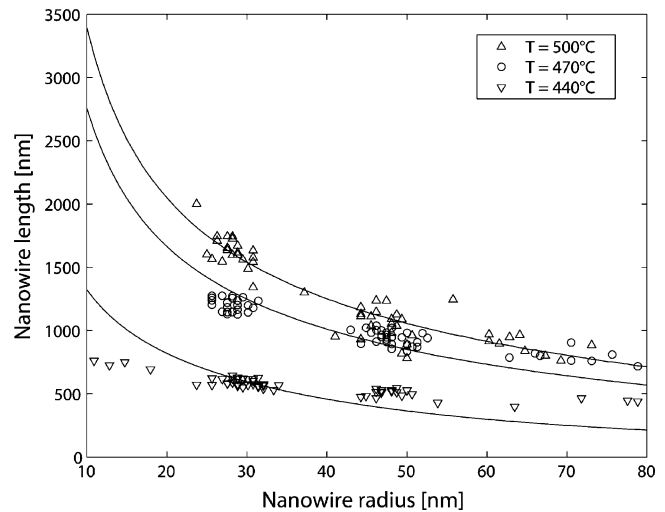


**Figure 3.** Model (solid curves) fitted to experimental values ( $\nabla$  440 °C,  $\circ$  470 °C, and  $\triangle$  500 °C).

versus the radii at all three temperatures. The solid curves result from combining eq 6 with eq 5, followed by integration from 0 to  $L$  and from 0 to the growth time. This gives  $L$  as a function of  $r_w$ . As the wires grow perpendicularly to the (111)B surface, the sides of the nanowires correspond to  $\{110\}$  facets. Thus,  $\lambda_s$  corresponds to diffusion on the substrate surface, and  $\lambda_w$  corresponds to diffusion along the nanowire sides. Gallium adatom diffusion on GaP surfaces, which is the main vehicle of mass transport in this study, is a poorly investigated system, and no values for the diffusion lengths could be obtained from the literature. Therefore, as a first attempt, we set  $\lambda_s = \lambda_w$  and treated this as a fitting parameter, which is the only free parameter in the model. The curves in Figure 3 were obtained by setting the diffusion lengths to 350 nm at 500 °C, 300 nm at 470 °C, and 250 nm at 440 °C. These are reasonable values corresponding to an activation energy for adatom migration of about 0.5 eV. By comparing these diffusion lengths with the interwire separations (Figure 2), we also see that assumption iv in the previous section (interwire separation larger than  $\lambda_s$ ) is indeed valid for the vast majority of the nanowires.

Moreover, these diffusion lengths are on the same order of magnitude as the InAs (111)B diffusion length of 650 nm at 440 °C estimated from CBE growth of nanowires.<sup>11</sup> The main discrepancy between the results in the present study and the work by Jensen et al.<sup>11</sup> is the diffusion length on the {110} side facets of the nanowires. Jensen et al. estimated this diffusion length to exceed 10  $\mu\text{m}$ , while we produce good fits with  $\lambda_w = \lambda_s$  which is much shorter. The explanation of this is that CBE is a high-vacuum beam technique where there is virtually no impingement on the nanowire sides ( $R_w \approx 0$  in CBE). This effect, in combination with the indications that in CBE the precursor molecules are not completely cracked until they reach the incorporation site,<sup>18</sup> will result in extremely long diffusion lengths. In MOVPE, however, the precursors are cracked to a greater extent before they attach to the surface, and the V/III ratio is much higher than that in CBE, which should lead to shorter diffusion lengths. We have shown that it is possible to produce similar fits with decreased  $\lambda_s$  and increased  $\lambda_w$ , which might reflect a more realistic situation. But due to the aforementioned lack of diffusion length data in the literature and the disadvantage of introducing an additional free parameter, we did not pursue this line of investigation. It should, however, be noted that  $L$  decreases with increasing  $r_w$  for all values of  $\lambda_s$  and  $\lambda_w$ , which is one of the main aspects of this model.

In MOVPE, the impingement occurs from a vapor surrounding the nanowires; therefore, we may write  $R = R_s = R_w = R_{\text{top}}$ . However, nanowire growth in MOVPE takes place at such low temperatures that the cracking of the group III precursors is incomplete. We know that our TMG flow corresponds to a nominal attachment rate for planar film growth of 0.5 ML/s (monolayers per second) when almost all the TMG is cracked. To estimate the attachment rate at the lower temperatures, we used the results of Larsen et al.<sup>19</sup> concerning the fraction of cracked TMG versus temperature in  $\text{H}_2$  ambient. This resulted in the following attachment rates: 0.5 ML/s at 500 °C, 0.48 ML/s at 470 °C, and 0.20 ML/s at 440 °C.

In Figure 3, we see that the model fits best to the high-temperature experimental data. The reason that it does not fit the data at 440 °C so well could be that mass transport might not be the only limiting process here. Instead, interface reactions, i.e., the kinetics of the incorporation of Ga and P into the nanowire, could become more important. This effect would indeed weaken the  $r_w$  dependence of  $L$ . Generally, film growth in chemical vapor deposition (CVD) is mass-transport-limited at high temperatures and surface-reaction-limited at low temperatures. Another effect that is not included in the model is the short time lag in the beginning of the growth, before the gold particle is supersaturated by growth species. During this time, growth is slower than predicted by the model.

It should also be noted that the model fits best to straight, i.e., untapered nanowires, as our GaP wires, which have a radius dictated by the assisting metal particle. In some systems, extensive materials incorporation on the nanowire sides occurs, which leads to tapered wires. In such systems, the adatoms that diffuse up along the wire, but do not reach the top, would incorporate into the wire side. However, in a first approximation to model such a system, two different radii have to be considered, the (time-dependent) radius at the base, which replaces  $r_w$  in eq 5, and the smaller top radius, equal to the metal particle radius, which is the same as the (explicit)  $r_w$  in eq 6. Since  $K_1(x)/K_0(x)$  decreases with increasing  $x$  (cf. eqs 5 and 6), the model in its present formulation slightly overestimates the length growth rate of significantly tapered wires.

It is easy to generalize our model to include the Gibbs–

Thomson effect, which could be in effect when the metal particle is small and/or when the supersaturation is low. In this case, we have to modify the attachment rate in the following way

$$R(r_w) = \frac{P - P_\infty \exp(2\sigma\Omega_1/r_w k_B T)}{\sqrt{2\pi m k_B T}} \quad (8)$$

This is the Hertz–Knudsen equation combined with the Gibbs–Thomson effect. The surrounding Ga pressure is denoted  $P$ , and the second term on the right-hand side describes how the pressure inside the metal particle increases with decreasing size,  $r_w$ . This term describes the Gibbs–Thomson effect where  $P_\infty$  is the Ga pressure inside a large (infinite curvature) metal particle,  $\sigma$  is the surface energy density of a large metal particle,  $\Omega_1$  is the atomic volume of Ga inside the metal particle,  $k_B T$  is the thermal energy, and  $m$  is the mass of a Ga atom.

We will show, using a numerical example, that the Gibbs–Thomson effect is not in operation during the growth of III/V nanowires at typical temperatures and reactant pressures. In our experiments at 470 °C,  $R = 0.48$  ML/s, which according to the Hertz–Knudsen equation corresponds to a Ga pressure of  $P = 2.76 \times 10^{-4}$  Pa. We now estimate the vapor pressure of pure liquid Ga at 470 °C, which we denote as  $P^*$ . To do this, we use the Clausius–Clapeyron equation<sup>20</sup> with  $\Delta H_{\text{vap}} = 258.7$  kJ/mol and the reference values  $P_0 = 9.31 \times 10^{-36}$  Pa at  $T_0 = 302.9$  K. This gives  $P^* = 2.48 \times 10^{-9}$  Pa at 470 °C. Given that the atomic fraction of Ga in the Au particle is about  $x = 0.1$ ,<sup>8</sup> we use Raoult's<sup>20</sup> law to obtain  $P_\infty = 2.48 \times 10^{-10}$  Pa, making the crude approximation that the activity coefficient is unity. If we approximate the surface energy of the Au–Ga metal particle to that of pure Au, which is about  $\sigma = 1.2$  N/m, then we obtain  $2\sigma\Omega_1/r_w k_B T = 3.97/r_w$ , where  $r_w$  is in nanometers. If  $R$  is to decrease by at least 10% due to the Gibbs–Thomson effect (eq 8), then this requires that  $r_w \leq 0.34$  nm, which is unreasonably small. Correspondingly, for  $R = 0$ , we would have  $r_w \leq 0.28$  nm. This example shows that the Gibbs–Thomson effect is not involved when growing metal-particle-assisted III/V nanowires at conventional supersaturations. However, when the supersaturation is very low, i.e., when  $P$  and  $P_\infty$  are on the same order of magnitude, as may be the case when growing Si wires from  $\text{SiCl}_4$ ,<sup>5,6,21</sup> the Gibbs–Thomson effect could be dominating. Due to the irreversibility of the TMG decomposition, it is not possible to reach low enough Ga pressures in a controllable manner in MOVPE such that the Gibbs–Thomson effect could be investigated for GaP nanowires.

As an example, we compare gold-particle-assisted silicon nanowire growth in two different Si systems. Schubert et al.<sup>10</sup> have grown nanowires with MBE at 525 °C, with a nominal Si beam flux corresponding to 0.5  $\text{\AA}/\text{s}$  (for two-dimensional growth), whereas Givargizov<sup>6</sup> and Wagner<sup>5</sup> have grown wires at around 1000 °C by atmospheric pressure CVD, using  $\text{SiCl}_4$  in  $\text{H}_2$  as the source. Schubert et al. observed the same trend as we do, i.e., that thinner nanowires grow faster than thicker ones, whereas Givargizov observed the opposite trend. How can this be explained? Givargizov based his model on the Gibbs–Thomson effect but without *explicitly* including the two pressures involved in this effect in his model, the partial Si pressure in the vapor and the partial pressure of Si in the metal alloy particle,  $P$  and  $P_\infty$ , respectively, in eq 8. It is here that the explanation is to be found. Starting with Schubert's experiment, we obtain from the Hertz–Knudsen equation,  $P = 4.9 \times 10^{-3}$  Pa for 525 °C and  $R = 0.5$   $\text{\AA}/\text{s}$ . The vapor pressure of Si at the same temperature is about  $P^* = 10^{-13}$  Pa. Since the atomic fraction of Si in the Au–Si alloy particle is around 0.5<sup>5</sup> and we

are only interested in the order of magnitude, we approximate  $P_\infty \approx P^* = 10^{-13}$  Pa. We note that  $P$  and  $P_\infty$  differ by 10 orders of magnitude, and thus we can neglect the second term on the right-hand side of eq 8 (compare the numerical example for Ga above), i.e., for this case the Gibbs–Thomson effect can be neglected.

Givargizov's experiments were conducted at 1050°C with molar percentages of SiCl<sub>4</sub> in H<sub>2</sub> ranging from 0.3 to 3.0. From these data, we crudely extrapolate a silicon pressure in the range  $P = 10^{-4}$ – $10^{-3}$  Pa, using the thermodynamic calculations of Langlais et al.<sup>22</sup> As the vapor pressure of Si at 1050 °C is about  $P^* = 10^{-5}$  Pa, we use the same approximation as above,  $P_\infty \approx 10^{-5}$  Pa. Now,  $P$  and  $P_\infty$  differ only by 1 order of magnitude, which implies that the second term on the right-hand side of eq 8, the Gibbs–Thomson effect, starts to become effective, and in this case, thinner wires grow slower than thicker ones, as was observed in Givargizov's experiments.

### Conclusions

We have presented a mass transport model for metal-particle-assisted nanowire growth. This model consists of two coupled surface diffusion equations, one for adatom diffusion on the substrate surface and the other for adatom diffusion along the side of the nanowire sidewalls. The nanowire growth rate is given by the adatom flux toward the top of the nanowire plus the direct impingement rate on the metal particle.

This model explains the common experimental observation that thinner metal-particle-assisted III/V nanowires are longer than thicker ones (when grown at the same temperature and with the same supply of material). We compared our model calculations with lengths and radii of MOVPE-grown GaP nanowires and found good agreement.

In addition to this, we demonstrated that the Gibbs–Thomson effect can be neglected when growing III/V nanowires at conventional temperatures and pressures, but that it can dominate in the SiCl<sub>4</sub>/H<sub>2</sub> system, which operates at much lower supersaturations.

**Acknowledgment.** This work was carried out within the Nanometer Structure Consortium in Lund and was supported

by grants from the Swedish Research Council, the Swedish Foundation for Strategic Research, and the NoE SANDiE (EU Grant No. NMP4-CT-2004 500101). We thank Lisa Karlsson for excellent TEM measurements.

### References and Notes

- (1) Haraguchi, K.; Katsuyama, T.; Hiruma, K.; Ogawa, K. *Appl. Phys. Lett.* **1992**, *60*, 745.
- (2) Cui, Y.; Lieber, C. M. *Science* **2001**, *291*, 851.
- (3) Björk, M. T.; Ohlsson, B. J.; Thelander, C.; Persson, A. I.; Deppert, K.; Wallenberg, L. R.; Samuelson, L. *Appl. Phys. Lett.* **2002**, *81*, 4458.
- (4) Thelander, C.; Mårtensson, T.; Björk, M. T.; Ohlsson, B. J.; Larsson, M. W.; Wallenberg, L. R.; Samuelson, L. *Appl. Phys. Lett.* **2003**, *83*, 2052.
- (5) Wagner, R. S., *Whisker Technology*. In *Whisker Technology*; Levitt, A. P., Ed.; Wiley: New York, 1970; pp 47–119.
- (6) Givargizov, E. I. *J. Cryst. Growth* **1975**, *31*, 20.
- (7) Kamins, T. I.; Williams, R. S.; Basile, D. P.; Hesjedal, T.; Harris, J. S. *J. Appl. Phys.* **2001**, *89*, 1008.
- (8) Persson, A. I.; Larsson, M. W.; Stenström, S.; Ohlsson, B. J.; Samuelson, L.; Wallenberg, L. R. *Nat. Mater.* **2004**, *3*, 677.
- (9) Dick, K.; Deppert, K.; Mårtensson, T.; Mandl, B.; Samuelson, L.; Seifert, W. *Nano Lett.* **2005**, *5*, 761.
- (10) Schubert, L.; Werner, P.; Zakharov, N. D.; Gerth, G.; Kolb, F. M.; Long, L.; Gösele, U.; Tan, T. Y. *Appl. Phys. Lett.* **2004**, *84*, 4968.
- (11) Jensen, L. E.; Björk, M. T.; Jeppesen, S.; Persson, A. I.; Ohlsson, B. J.; Samuelson, L. *Nano Lett.* **2004**, *4*, 1961.
- (12) Seifert, W.; Borgström, M.; Deppert, K.; Dick, K. A.; Johansson, J.; Larsson, M. W.; Mårtensson, T.; Sköld, N.; Svensson, C. P. T.; Wacaser, B. A.; Wallenberg, L. R.; Samuelson, L. *J. Cryst. Growth* **2004**, *272*, 211.
- (13) Magnusson, M. H.; Deppert, K.; Malm, J. O.; Bovin, J. O.; Samuelson, L. *J. Nanopart. Res.* **1999**, *1*, 243.
- (14) Borgström, M.; Deppert, K.; Samuelson, L.; Seifert, W. *J. Cryst. Growth* **2004**, *260*, 18.
- (15) Björk, M. T.; Ohlsson, B. J.; Sass, T.; Persson, A. I.; Thelander, C.; Magnusson, M. H.; Deppert, K.; Wallenberg, L. R.; Samuelson, L. *Appl. Phys. Lett.* **2002**, *80*, 1058.
- (16) Joyce, B. A.; Neave, J. H.; Zhang, J.; Vvedensky, D. D.; Clarke, S.; Hugill, K. J.; Shitara, T.; Myersbeaghton, A. K. *Semicond. Sci. Technol.* **1990**, *5*, 1147.
- (17) Abramowitz, M.; Stegun, I. A. *Handbook of Mathematical Functions With Formulas, Graphs, and Mathematical Tables*, 10th ed.; United States Department of Commerce: Washington, DC, 1972.
- (18) Jeppesen, S. Private communication.
- (19) Larsen, C. A.; Buchan, N. I.; Li, S. H.; Stringfellow, G. B. *J. Cryst. Growth* **1990**, *102*, 103.
- (20) Atkins, P. W., *Physical Chemistry*, 4th ed.; Oxford University Press: Oxford, U. K., 1990.
- (21) Wu, Y. Y.; Fan, R.; Yang, P. D. *Nano Lett.* **2002**, *2*, 83.
- (22) Langlais, F.; Hottier, F.; Cadoret, R. *J. Cryst. Growth* **1982**, *56*, 659.